Amphiphilic peroxynitrite decomposition catalysts in liposomal assemblies

Julianne A Hunt, Jinbo Lee and John T Groves

Background: Peroxynitrite ($ONOO^-$), a toxic biological oxidant, has been implicated in many pathophysiological conditions. The water-soluble porphyrins 5,10,15,20-tetrakis(*N*-methyl-4′-pyridyl)porphinato iron(III) (FeTMPyP) and manganese(III) (MnTMPyP) have recently emerged as potential drugs for $ONOO^-$ detoxification, and FeTMPyP has demonstrated activity in models of $ONOO^-$ related disease states. We set out to develop amphiphilic analogs of FeTMPyP and MnTMPyP suitable for liposomal delivery in sterically stabilized liposomes (SLs).

Results: Three amphiphilic iron porphyrins (termed **1a–c)** and three manganese porphyrins (termed **2a–c)** bound to liposomes and catalyzed the decomposition of $ONOO^-$. The polyethylene-glycol-linked metalloporphyrins **1b** and **2b** proved the most effective of these catalysts, rapidly decomposing $ONOO^-$ with second-order rate constants (k_{cat}) of $2.9 \times 10^5\ M^{-1}\ s^{-1}$ and $5.0 \times 10^5\ M^{-1}\ s^{-1}$, respectively, in dimyristoylphosphatidylcholine liposomes. Catalysts **1b** and **2b** also bound to SLs, and these metalloporphyrin–SL constructs efficiently catalyzed $ONOO^-$ decomposition ($k_{cat} \approx 2 \times 10^5\ M^{-1}\ s^{-1}$). The analogous metalloporphyrins **1a** and **2a**, which are not separated from the vesicle membrane surface by polyethylene glycol linkers, were significantly less effective ($k_{cat} \approx 3.5 \times 10^4\ M^{-1}\ s^{-1}$).

Conclusions: For these amphiphilic analogs of FeTMPyP and MnTMPyP, the polarity of the environment of the metalloporphyrin headgroup is intimately related to the efficiency of the catalyst; a polar aqueous environment is essential for effective catalysis of $ONOO^-$ decomposition. Thus, catalysts **1b** and **2b** react rapidly with $ONOO^-$ and are potential therapeutic agents that, unlike their water-soluble TMPyP analogs, could be administered as liposomal formulations in SLs. These SL-bound amphiphilic metalloporphyrins may prove to be highly effective in the exploration and treatment of $ONOO^-$ related disease states.

Address: Department of Chemistry, Princeton University, Princeton, NJ 08544, USA.

Correspondence: John T Groves
E-mail: jtgroves@princeton.edu

Key words: membrane self-assembly, metalloporphyrins, peroxynitrite, sterically stabilized liposomes

Received: **21 August 1997**
Revisions requested: **15 September 1997**
Revisions received: **22 September 1997**
Accepted: **23 September 1997**

Chemistry & Biology November 1997, 4:845–858
http://biomednet.com/elecref/1074552100400845

Introduction

Peroxynitrite ($ONOO^-$) is a potent oxidant formed by the direct and rapid combination of nitric oxide and the superoxide anion ($O_2^{-\bullet}$) [1–3]. $ONOO^-$ crosses lipid membranes at a rate significantly faster than the rates of its known decomposition pathways [4], indicating that this oxidant, unlike reactive radicals such as $O_2^{-\bullet}$ or $HO^\bullet$, can travel distances of cellular dimensions. Thus, even in the presence of biological membranes, $ONOO^-$ should have free access to cell interiors. $ONOO^-$ is known to nitrate tyrosine residues in proteins [5,6], and to oxidize metalloenzymes [7,8], DNA [9,10], lipids [11], sulfhydryls [12] and methionines [13]. In light of this reactivity, $ONOO^-$ has been implicated in a host of disease states, including neurodegenerative disorders such as Alzheimer's disease [13–17], amyotrophic lateral sclerosis [18–21], stroke [22–24], AIDS dementia [25] and Huntington's disease [26]; heart diseases such as atherosclerosis [27]; chronic inflammation and autoimmune diseases such as arthritis [28], inflammatory bowel disease [29,30] and acute respiratory disease syndrome [31]; and cancer [32–34], ischemia-reperfusion injury [1,35,36], septic shock [37] and chronic rejection of renal allografts [38].

This large and growing body of evidence for the major role of $ONOO^-$ in a wide variety of human diseases has naturally led to a search for drugs that can detoxify the powerful oxidant, and a family of synthetic, water-soluble porphyrins has emerged as potential candidates [39–41]. Stern and co-workers [40] discovered that the iron porphyrins 5,10,15,20-tetrakis(*N*-methyl-4′-pyridyl)-porphinatoiron(III) (FeTMPyP) and 5,10,15,20-tetrakis (2,4,6-trimethyl-3,5-sulfonatophenyl)porphinatoiron(III) (FeTMPS) catalyze the efficient decomposition of $ONOO^-$ to NO_3^- under physiological conditions. These iron porphyrins have profound activity in biological models of $ONOO^-$ related disease states and have been investigated as therapeutic agents for diseases in which $ONOO^-$ has been implicated [40,42,43].

We have shown that $ONOO^-$ reacts rapidly and stoichiometrically with the water-soluble synthetic manganese porphyrin 5,10,15,20-tetrakis(*N*-methyl-4′-pyridyl)porphinato manganese(III) (MnTMPyP) to generate oxomanganese intermediates [39,44]. Further, MnTMPyP catalyzed the rapid reduction of $ONOO^-$ in the presence of common biological reducing agents such as ascorbate, Trolox® (a water-soluble analog of α-tocopherol), and glutathione (Figure 1) [45]. In addition to this 'peroxynitrite reductase' activity, MnTMPyP has previously been shown to possess significant superoxide dismutase (SOD) activity *in vitro* and to protect cells from oxidative stress; however, it is significant that the scavenging of $O_2^{-\bullet}$ alone could not fully explain the cell-protective effects of MnTMPyP in a SOD-null strain of *Escherichia coli* [46]. Finally, the synthetic manganese porphyrin 5,10,15,20-tetrakis(4-benzoic acid)porphinato manganese(III) (MnTBAP) has demonstrated pharmacological efficacy in $ONOO^-$ related disease models [41,47]. In combination, these experiments point to the potential use of MnTMPyP and related manganese complexes for pharmaceutical intervention in pathological processes related to both $O_2^{-\bullet}$ and $ONOO^-$.

In light of the therapeutic possibilities of FeTMPyP, MnTMPyP and related metal complexes, we have sought to design amphiphilic analogs of these water-soluble metalloporphyrins that would retain catalytic activity when placed in phospholipid vesicular assemblies [48]. Liposomes are attractive vehicles for the delivery of chemotherapeutic agents: the drugs can be encapsulated in the aqueous interior volumes or incorporated in the lipid membranes of the liposomes and transported to target cells without the need for covalent bonding between the drug and the targeting ligand. During transport, liposomes can protect the incorporated drug from metabolic degradation while protecting non-target cells from the drug [49]. The recent development of sterically stabilized liposomes with enhanced biological stability has revitalized the prospects for the use of liposomes as drug carriers; these liposomes avoid rapid uptake by the phagocytic molecules of the reticuloendothelial system (primarily the liver and spleen) and thus have long blood circulation times [50–52].

Figure 1

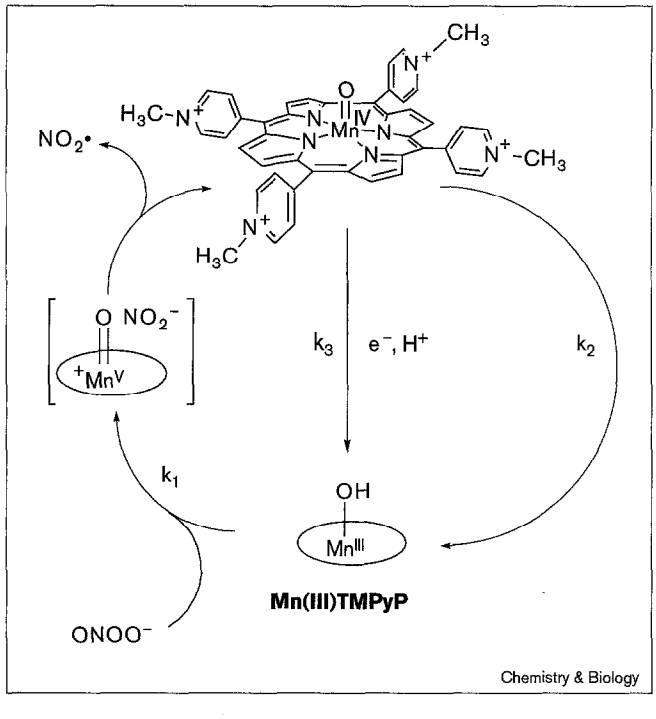

Reduction of $ONOO^-$ by MnTMPyP. Rate constants: $k_1 = 1.8 \times 10^6$ $M^{-1} s^{-1}$; $k_2 = 0.018$ s^{-1}; $k_3 = 5.4 \times 10^7$ $M^{-1} s^{-1}$ for ascorbate; $k_3 = 1.3 \times 10^5$ $M^{-1} s^{-1}$ for glutathione; $k_3 = 7.0 \times 10^6$ $M^{-1} s^{-1}$ for Trolox®.

We report herein the development of new membrane-bound metalloporphyrin catalysts of $ONOO^-$ decomposition that are amenable to liposomal drug delivery, and we have demonstrated the compatibility of these catalytic systems with sterically stabilized liposomes.

Results and discussion

Design strategies

We sought to develop a vesicle-bound agent for the catalytic decomposition of $ONOO^-$ in order to exploit the advantages of liposomal drug-delivery systems. Thus, we set out to design an amphiphilic or hydrophobic metalloporphyrin-based catalyst which could reasonably be expected to react rapidly with $ONOO^-$. Because the rates of reaction of the metalloTMPyPs with $ONOO^-$ ($\sim 2 \times 10^6$ $M^{-1}s^{-1}$) are among the highest known for this oxidant [39,40,44], we anticipated that amphiphilic analogs of TMPyP, such as FeAmPEGTPyP (**1b**) and MnAmPEGTPyP (**2b**; Figure 2), would be excellent choices for porphyrin-based, membrane-bound $ONOO^-$ decomposition catalysts.

The first step in our design strategy, however, was to evaluate extant membrane-binding metalloporphyrins for catalytic $ONOO^-$ decomposition activity. Several families of membrane-associated metalloporphyrins for the construction of self-assembling, multicomponent membrane ensembles have been described previously, and these constructs have demonstrated various forms of catalytic and electron-transfer activity [48,53,54]. Figure 3 shows a few of these porphyrins, including 5,10,15,20-tetrakis(2,4,6-trimethylphenyl)porphinatoiron (III) (FeTMP), α,β,α,β-*meso*-[tetra(*o*-3β-hydroxy-5-cholenylamidophenyl]porphinatoiron(III) (FeChP), and 5,10,15-*meso*-[tris(*p*-carboxyphenyl))-20-(octadecylphenyl)]-porphinatoiron(III) (FeTCAmP). Phospholipid vesicles, which form the membrane-mimetic matrix for the assembly of these porphyrins into multicomponent systems, can be divided into a number of discrete regions distinguished by their polarity (e.g., the aqueous interior

Figure 2

Amphiphilic polyethylene glycol-3 (PEG-3)-linked $ONOO^-$ decomposition catalysts. The lipophilic dodecyl 'legs' of the molecule anchor it in one leaflet of the membrane bilayer, while the hydrophilic PEG-3 linkers allow the positively charged porphyrin macrocycle to extend into the external aqueous solvent. The pink ball in the center of the porphyrin macrocycle represents the bound metal, Fe in compound **1b** or Mn in compound **2b**.

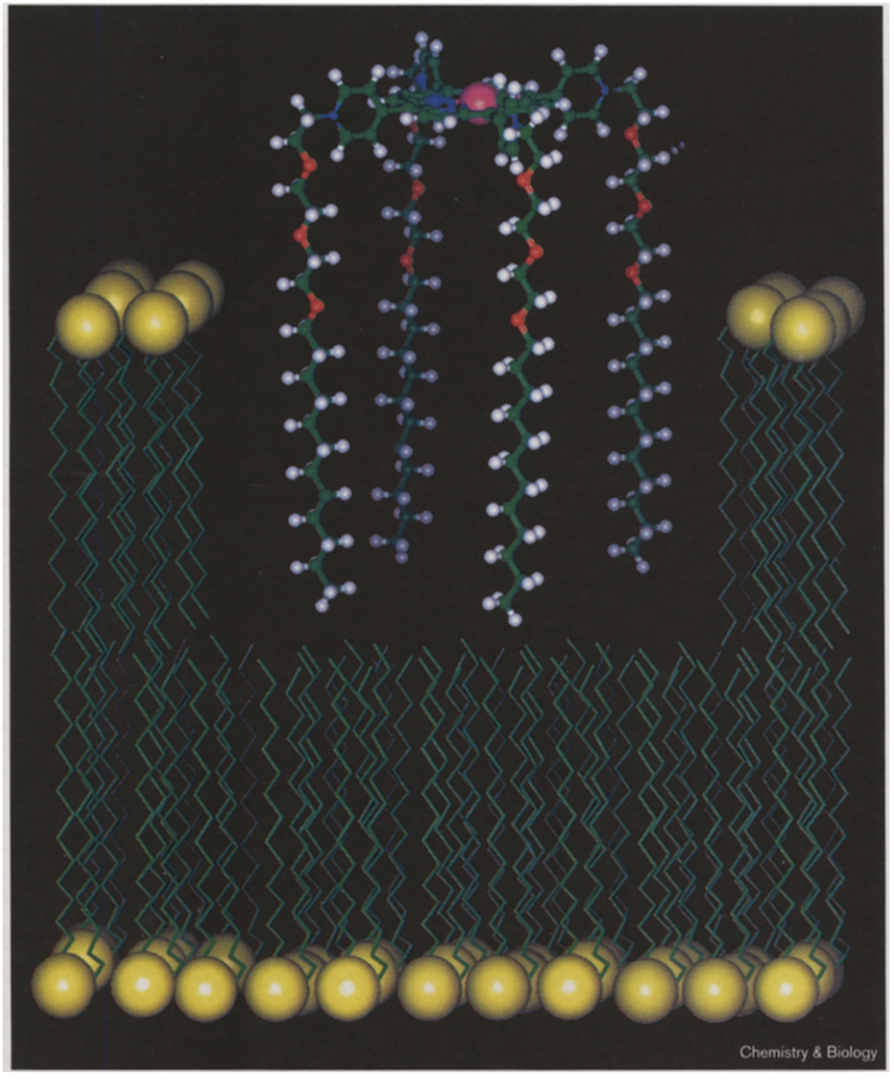

volume, the hydrophobic membrane bilayer, the outer hydration sphere and the aqueous bulk solvent) [55]; therefore, vesicles allow for assembly of components on the basis of their polarity. The three iron porphyrins shown in Figure 3 are thus localized by their polarity in specific regions of the vesicle bilayers: the tetramesityl porphyrin FeTMP is located in the hydrophobic interior of the vesicle; the steroidal porphyrin FeChP [53] spans the bilayer membrane as shown, with the metalloporphyrin macrocycle located in the middle of the bilayer; and the amphiphilic tricarboxy porphyrin FeTCAmP [48,56] is anchored in the membrane by its single lipophilic tail, with its metalloporphyrin headgroup located at the surface of the membrane, at the interface between the membrane and the bulk aqueous solvent.

These three membrane-bound iron porphyrins were evaluated for catalytic $ONOO^-$ decomposition activity, but the presence of these compounds did not affect the rate of $ONOO^-$ decay; only spontaneous decay of peroxynitrite was observed [57]. That is, none of these porphyrins proved to be efficient $ONOO^-$ decomposition catalysts. The hydrophobic environment of FeChP and FeTMP is most likely to be responsible for the slow rates of reaction of these compounds with the hydrophilic $ONOO^-$, but the lack of catalytic activity of the amphiphilic porphyrin FeTCAmP was more puzzling. Examination of the catalytic activity of 5,10,15,20-tetrakis(4-benzoic acid)porphine (TBAP), however, which is the water-soluble 'parent' of the amphiphilic FeTCAmP, proved that the parent porphyrin catalyzes $ONOO^-$ decomposition at a surprisingly slow rate ($k_{cat} = 5 \times 10^4\ M^{-1}s^{-1}$; data not shown). Although this rate precludes the porphyrin from demonstrating efficient catalytic activity at low concentrations, it is consistent with the observations by Szabo and coworkers [47] that MnTBAP is an effective scavenger of $ONOO^-$ at high

Figure 3

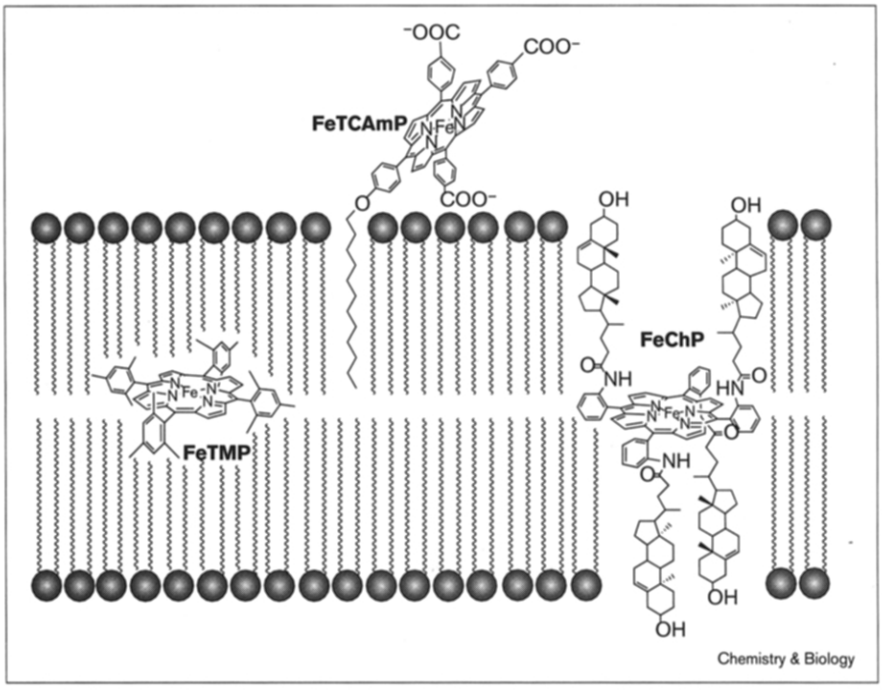

Membrane-associated iron porphyrins. FeTMP is located in the hydrophobic interior of the vesicle, FeTCAmP is anchored in the membrane by a lipophilic tail, with the metalloporphyrin headgroup located in the interface between the membrane and the aqueous solvent, and FeChP spans the membrane bilayer, with the metalloporphyrin macrocycle located in the middle of the bilayer.

concentrations. Given the slow reaction of its parent porphyrin with $ONOO^-$, FeTCAmP would not be expected to show significant catalytic $ONOO^-$ decomposition activity.

Finally, we turned to the preparation of amphiphilic analogs of the fast $ONOO^-$ decomposition catalysts FeTMPyP and MnTMPyP, armed with the knowledge that the best candidates for amphiphilic $ONOO^-$ decomposition catalysts would reside in a hydrophilic environment. As depicted in Figure 2, we envisaged that, in liposomal preparations, the highly charged tetrapyridinium porphyrin macrocycles of these amphiphilic compounds would reside at the interface between the lipid membrane and the bulk aqueous solution, while the four lipophilic sidechains would be firmly anchored in the hydrophobic bilayer.

Although metalloporphyrins **1a** and **2a** (see Figures 4 and 5 for the structures of all six amphiphilic TMPyP analogs), with their simple dodecyl sidechains, proved the easiest amphiphilic TMPyP analogs to synthesize and characterize, our expectation that a hydrophilic environment for the metalloporphyrin headgroup would prove to be necessary for the efficiency of the catalysts prompted us to prepare the polyethylene glycol (PEG)-linked porphyrins **1b–c** and **2b–c**. The PEG linkers of compounds **1b–c** and **2b–c** were added to extend the porphyrin headgroup further out of the interfacial region between the membrane and the external solution and further into the bulk solvent. We found that the hydrophilicity of the environment of the porphyrin headgroup correlated very well with the efficiency of the catalysts: the rate of $ONOO^-$ decomposition catalyzed by the PEG-linked metalloporphyrins was an order of magnitude faster than the rate of $ONOO^-$ decomposition catalyzed by the metalloporphyrins with simple dodecyl chains. This remarkable discrepancy in the activity of these structurally similar catalysts demonstrated that incorporation of the PEG linkers was indeed essential for the successful design of effective $ONOO^-$ decomposition catalysts; at low catalyst concentrations (~10 μM) the simple tetradodecylpyridinium metalloporphyrins did not significantly increase the rate of $ONOO^-$ decomposition, while the PEG-linked metalloporphyrins at the same concentrations enhanced the rate of $ONOO^-$ decomposition at least tenfold.

Synthesis of the amphiphilic catalysts and preparation of vesicles

The pyridinium porphyrins **6a–c** used in these studies were synthesized, as shown in Figure 4, by peralkylation of 5,10,15,20-tetrakis(4-pyridyl)porphine (TPyP, **5**) with the appropriate alkyl iodide [58]: dodecyl iodide is commercially available, while iodides **4a** and **4b** were prepared by direct iodination [59] of the corresponding commercially available alcohols **3a** and **3b**. H_2AmTPyP (**6a**), with four simple dodecyl sidechains, was prepared from TPyP in 90% yield; H_2AmPEGTPyP (**6b**), with the four dodecyl sidechains attached to the porphyrin macrocycle via PEG-3 spacers, was prepared in 94% yield; and H_2AmPEG_6TPyP (**6c**), with the dodecyl sidechains attached to the porphyrin

Figure 4

Synthesis of amphiphilic tetrapyridinium porphyrins from tetrapyridylporphine **(5)** and alkyl iodides.

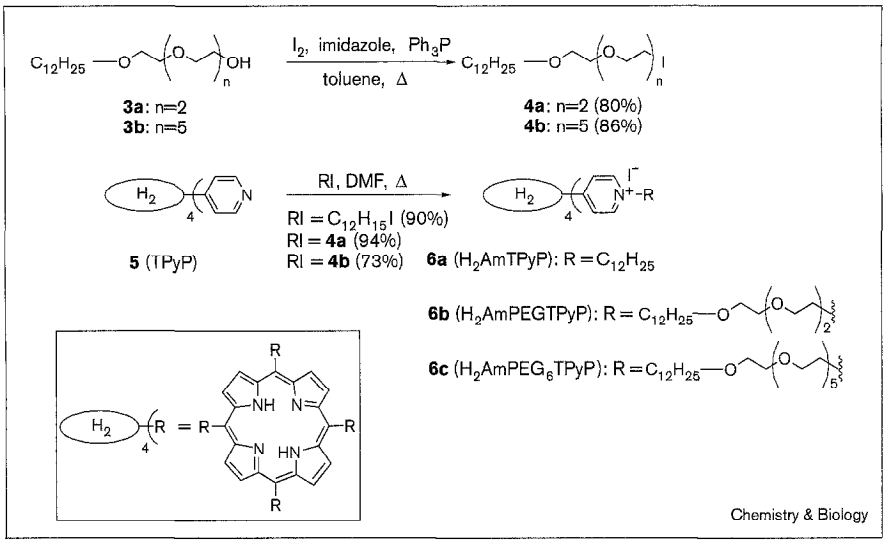

macrocycle via PEG-6 spacers, was prepared in 73% yield. The three amphiphilic iron porphyrins **1a–c** and three amphiphilic manganese porphyrins **2a–c** were then prepared in good yields from the corresponding amphiphilic free bases **6a–c** by metallation of the porphyrin macrocycles under standard conditions [53], as shown in Figure 5.

With the six amphiphilic porphyrins in hand, we prepared suspensions of small unilamellar vesicles doped with the porphyrins **1a–c** and **2a–c** by sonication of thin films of lipid–porphyrin mixtures in phosphate buffer, as we have described previously [48,53]. Similarly, vesicular suspensions doped with the porphyrins **2a–c** and α-tocopherol were prepared by sonication of thin films of lipid–porphyrin–tocopherol mixtures in buffer. For experiments requiring ascorbate, vesicles were incubated with ascorbate for 30 min prior to using the vesicular suspensions, in order to allow the ascorbate to diffuse through the lipid membranes and into the interior aqueous compartments of the vesicles [60]. Finally, sterically stabilized small unilamellar vesicles doped with porphyrin **1b** or porphyrin **2b** plus α-tocopherol were prepared by the same protocol, from thin films containing ~60 mol% dimyristoylphosphatidylcholine (DMPC), 30 mol% cholesterol and 5 mol% PEG-2000-dipalmitoylphosphatidylethanolamine (PEG-2000-DSPE).

Peroxynitrite decomposition by the iron porphyrins

We determined the rates of $ONOO^-$ decomposition catalyzed by vesicular suspensions of the amphiphilic iron porphyrins **1a–c** using stopped-flow spectrophotometry. We have previously shown that phospholipid vesicles are not disrupted under the conditions of the stopped-flow

Figure 5

Metallation of amphiphilic free-base porphyrins **6a–c** to provide iron porphyrins **1a–c** and manganese porphyrins **2a–c**.

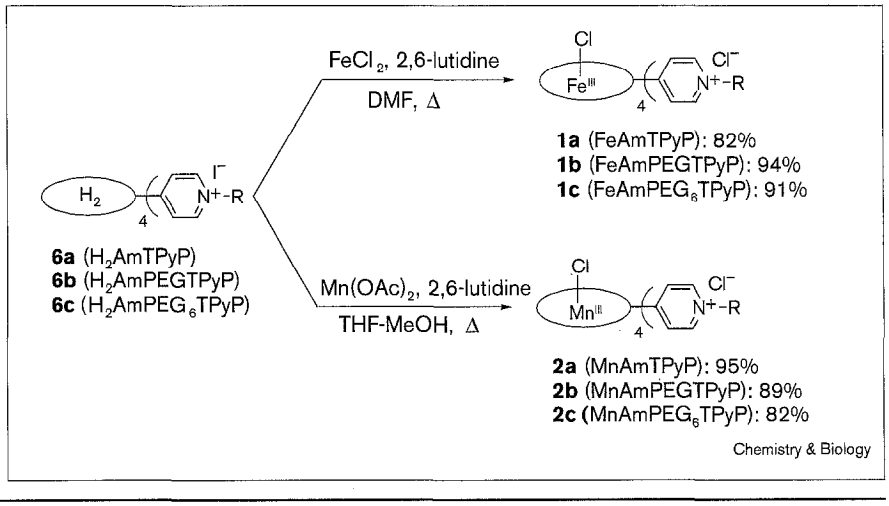

experiments [4]. The catalytic rate constants were measured by monitoring the disappearance of the strong $ONOO^-$ absorbance at 302 nm. Figure 6a shows typical traces for the decomposition of $ONOO^-$ in the absence of any porphyrin, with a self-decay rate constant $k_{self} = 0.26\ s^{-1}$ (trace i), and for the decomposition of $ONOO^-$ in the presence of iron porphyrins **1a** (trace ii), **1b** (trace iii) and **1c** (trace iv).

Figure 6

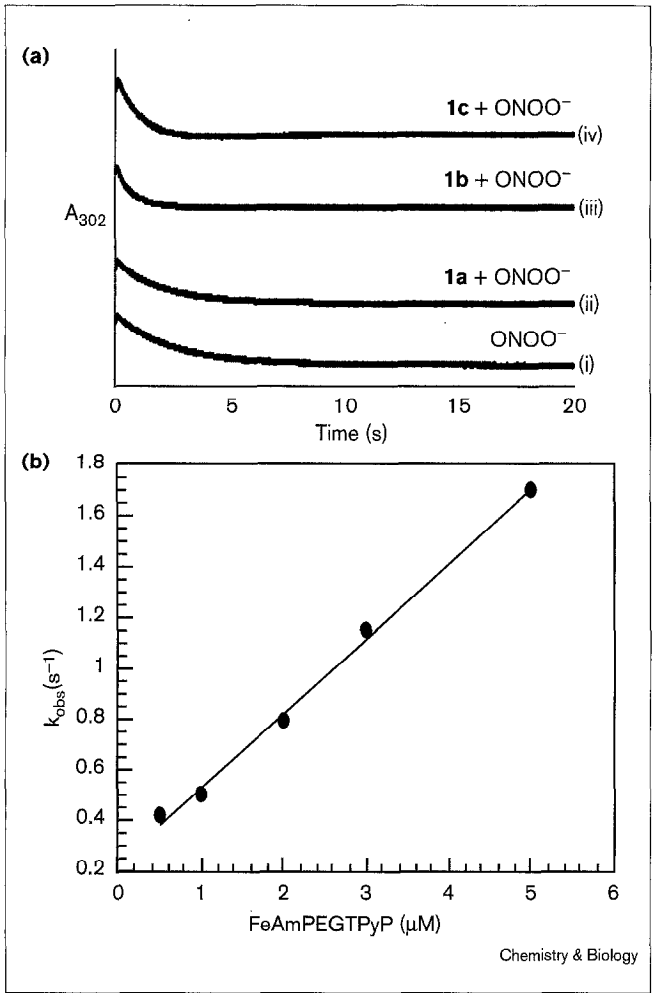

Typical kinetic profiles of the reactions of vesicular suspensions of iron porphyrins **1a–c** with $ONOO^-$. **(a)** Decomposition of $ONOO^-$ monitored at 302 nm, in the absence of porphyrin (trace i); and in the presence of 2.6 μM FeAmTPyP (**1a**; trace ii); 2.5 μM FeAmPEGTPyP (**1b**, trace iii); and 3 μM $FeAmPEG_6TPyP$ (**1c**, trace iv). The full scale corresponds to 0.8 OD. The background absorption due to porphyrin results in vertical displacement of traces (ii), (iii) and (iv) relative to (i). The position of trace (ii) reflects this normal vertical displacement, while traces (iii) and (iv) have been additionally offset for convenience. **(b)** Linear least-squares fitting of the pseudo-first order rates of decomposition of $ONOO^-$ (k_{obs}) versus FeAmPEGTPyP **(1b)** concentration. Each data point is the mean of 3–5 trials. Extrapolation of the line gives an intercept of $0.24\ s^{-1}$, which is consistent with the rate of self-decomposition of $ONOO^-$ under these conditions. The second-order rate constant, given by the slope of the line, is $2.9 \times 10^5\ M^{-1}\ s^{-1}$ ($R = 0.99819$).

The rate constants (k_{cat}) for the decomposition of $ONOO^-$ catalyzed by the amphiphilic iron porphyrins **1a–c** are shown in Table 1. These rate constants were determined via a series of stopped-flow kinetic experiments in which the initial $ONOO^-$ concentrations were held constant at 100 μM and the porphyrin concentrations were varied over a range of ~0.5 to 20 μM. As shown for FeAmPEGTPyP (**1b**) in Figure 6b, a plot of the pseudo-first-order rate constants (k_{obs}) so obtained versus catalyst concentrations provided the apparent first-order rates of $ONOO^-$ decomposition (k_{cat}) catalyzed by each of the three porphyrins.

Significantly, insertion of the PEG spacers in compounds **1b** and **1c** resulted in a large increase in the rate of $ONOO^-$ decomposition, as compared to the rate of decomposition catalyzed by FeAmTPyP. FeAmTPyP (**1a**), with its simple dodecyl sidechains, is a much less effective catalyst than either FeAmPEGTPyP (**1b**) or $FeAmPEG_6TPyP$ (**1c**). Also, while insertion of the PEG-3 spacer in FeAmPEGTPyP resulted in a dramatic increase in the rate of $ONOO^-$ decomposition, extension of the spacer to six PEGs in $FeAmPEG_6TPyP$ offered no further increase in rate. Clearly the catalyst functions more effectively when attachment of the PEG-3 linker enables it to extend out into the interface region between the vesicle surface and the bulk aqueous solution, but no further gain in catalytic efficiency is observed when the linker is doubled in length. We observed an analogous trend in catalytic efficiency versus linker composition in the manganese porphyrins **2a–c** (see below). Finally, it should be noted that, although the k_{cat} of the PEG-6-linked porphyrin **1c** was nearly identical to the k_{cat} of the PEG-3-linked analog **1b**, the PEG-6 porphyrin **1c** strongly promoted vesicle aggregation, making this catalyst less manageable than its PEG-3 analog **1b**.

Peroxynitrite reduction by the manganese porphyrins

The oxidation of MnTMPyP by $ONOO^-$ is fast ($k_1 = 1.8 \times 10^6\ M^{-1}s^{-1}$), producing oxoMn(IV)TMPyP and $NO_2^{\bullet}$ (see Figure 1), but Mn(III) porphyrins are poor catalysts for $ONOO^-$ decomposition because the first-order reduction of the oxoMn(IV) species back to the Mn(III) oxidation state is slow (k_2). However, we have recently demonstrated that MnTMPyP can catalyze the rapid reduction of $ONOO^-$ in the presence of biological reducing agents such as ascorbate ($k_{cat} = 2.2 \times 10^6\ M^{-1}s^{-1}$), glutathione ($k_{cat} = 3.2 \times 10^6\ M^{-1}s^{-1}$), and Trolox®, a water-soluble analog of α-tocopherol ($k_{cat} = 1.1 \times 10^6\ M^{-1}s^{-1}$) [45]. These agents rapidly reduce oxoMn(IV)TMPyP back to MnTMPyP (k_3), efficiently closing the catalytic cycle. We thus expected that the manganese analogs of the amphiphilic iron porphyrins **1a–c** described above would become active catalysts in the presence of biological reducing agents.

The rates of $ONOO^-$ reduction in the presence of vesicular suspensions of the amphiphilic manganese porphyrins **2a–c** were determined by monitoring the disappearance

Table 1

$ONOO^-$ decomposition catalysts.

Porphyrin	Fe catalyst	k_{cat} (M^{-1} s^{-1})	Mn catalyst	Reductant	k_{cat} (M^{-1} s^{-1})
TMPyP	FeTMPyP	2.2×10^{6}*	MnTMPyP	Ascorbate	2.2×10^{6}†
TMPyP			MnTMPyP	Trolox®	1.1×10^{6}†
TMPS	FeTMPS	6.5×10^{5}*			
AmPEGTPyP	**1b**	2.9×10^{5}	**2b**	Ascorbate	5.0×10^{5}
AmPEGTPyP	**1b**/ascorbate	3.3×10^{5}	**2b**	α-Tocopherol	4.6×10^{5}
AmPEGTPyP	**1b**/SLs‡	2.3×10^{5}	**2b**/SLs‡	α-Tocopherol	1.9×10^{5}
$AmPEG_6TPyP$	**1c**	2.0×10^{5}	**2c**	Ascorbate	1.8×10^{5}
AmTPyP	**1a**	4.0×10^{4}	**2a**	Ascorbate	3.3×10^{4}

*From [39]; †from [45]; ‡SLs, sterically stabilized liposomes.

of $ONOO^-$ at 302 nm by stopped-flow spectrophotometry. As with MnTMPyP, the manganese porphyrins **2a–c** showed poor catalytic activity in the absence of reducing agents: Figure 7a shows typical traces for the decomposition of $ONOO^-$ in the absence (trace i) of any porphyrin, and in the presence of Mn(III)AmPEGTPyP (**2b**, trace ii). While the presence of the porphyrin does decrease the half-life of $ONOO^-$ somewhat, the rate of $ONOO^-$ reduction catalyzed by **2b** is limited by the rate of reduction of oxoMn(IV)AmPEGTPyP back to the Mn(III) state, and is therefore much slower than the rate of $ONOO^-$ decomposition catalyzed by the analogous iron porphyrin **1b**.

However, the second-order rate of reaction of Mn(III)-AmPEGTPyP (**2b**) with $ONOO^-$ to provide oxoMn(IV)-AmPEGTPyP (measured by monitoring the disappearance of Mn(III)AmPEGTPyP at 462 nm or the concurrent appearance of oxoMn(IV) at 434 nm, as shown in Figure 7b) showed that the oxidation of **2b** compared well with the rate of $ONOO^-$ decomposition catalyzed by the analogous iron porphyrin **1b**: $k_1 = 3.6 \times 10^5\ M^{-1}s^{-1}$ for **2b**, while $k_{cat} = 2.9 \times 10^5\ M^{-1}s^{-1}$ for **1b**. Thus, we expected that porphyrins **2a–c** would efficiently catalyze the decomposition of $ONOO^-$ in the presence of the appropriate agents for rapidly reducing the amphiphilic oxoMn(IV) porphyrins to the corresponding Mn(III) porphyrins.

In the presence of ascorbate, the amphiphilic manganese porphyrins **2a–c** showed significant catalytic activity; in fact, the rates of $ONOO^-$ reduction catalyzed by the manganese porphyrins under these reducing conditions compared well with the rates of $ONOO^-$ decomposition catalyzed by the iron porphyrins (see Table 1). Figure 8a shows typical traces for the disappearance of $ONOO^-$ in the absence of any porphyrin (trace i), in the presence of ascorbate only (trace ii), and in the presence of manganese porphyrins **2a** (trace iii), **2b** (trace iv), and **2c** (trace v) plus 1.5 equivalents of ascorbate per equivalent of $ONOO^-$. Although ascorbate alone did participate in reduction of $ONOO^-$, the second-order rate of this process was slow ($k_2 = 236\ M^{-1}s^{-1}$) (see also [61,62]) compared to the porphyrin-catalyzed reduction. In a separate experiment, we also measured the rate of $ONOO^-$ decomposition catalyzed by FeAmPEGTPyP (**1b**) plus ascorbate, but we found no significant rate acceleration for the iron catalyst in the presence of this biological reducing agent (see Table 1). Clearly, the function of ascorbate in the manganese amphiporphyrin-catalyzed $ONOO^-$ reduction is the rapid reduction of the amphiphilic oxoMn(IV) species to the corresponding Mn(III) amphiporphyrins.

As with the iron porphyrins **1a–c**, MnAmPEGTPyP (**2b**) and $MnAmPEG_6TPyP$ (**2c**) are much more effective catalysts than MnAmTPyP (**2a**). The manganese porphyrins thus showed the same trend in catalytic efficiency versus linker composition that we observed for the iron porphyrins; that is, insertion of the PEG-3 spacer in MnAmPEGTPyP greatly increased the rate of catalytic $ONOO^-$ reduction, as compared to the rate of reduction catalyzed by MnAmTPyP, but insertion of the PEG-6 spacer in $MnAmPEG_6TPyP$ offered no further increase in rate. This analogous behavior of the amphiphilic iron and manganese porphyrins corroborates our conclusion that these catalysts function most effectively when allowed to extend into the interface region between the vesicle surface and the bulk aqueous solution. As with the iron porphyrin **1c**, the manganese porphyrin **2c** strongly promoted vesicle aggregation.

Remarkably, α-tocopherol also proved to be an excellent reducing agent for the oxomanganese(IV) amphiphilic porphyrins. In our previous experiments with the water-soluble MnTMPyP, we found that Trolox®, a water-soluble analog of α-tocopherol, rapidly reduced oxoMn(IV)TMPyP to Mn(III)TMPyP ($k_2 = 7.0 \times 10^6\ M^{-1}s^{-1}$). However, the lipid-soluble α-tocopherol (delivered as a vesicular suspension)

Figure 7

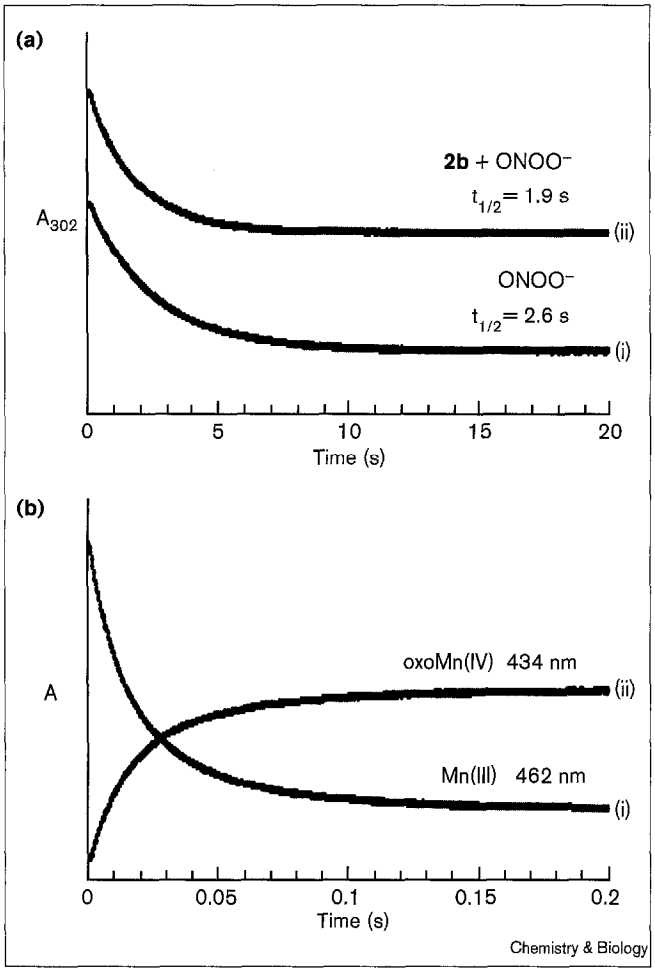

Typical kinetic profiles of the reaction of a vesicular suspension of MnAmPEGTPyP **(2b)** with $ONOO^-$. **(a)** Trace (i) shows the decomposition of $ONOO^-$ (100 μM), monitored at 302 nm, in the absence of porphyrin **2b**, and trace (ii) shows the decomposition of $ONOO^-$ (100 μM), monitored at 302 nm, in the presence of 2.5 μM **2b**. **(b)** Trace (i) shows the disappearance of Mn(III)AmPEGTPyP (7.5 μM) in the presence of $ONOO^-$ (100 μM), monitored at 462 nm, and trace (ii) shows the appearance of oxoMn(IV)AmPEGTPyP (7.5 μM) in the presence of $ONOO^-$ (100 μM), monitored at 434 nm. The full scale corresponds to 0.5 OD.

Figure 8

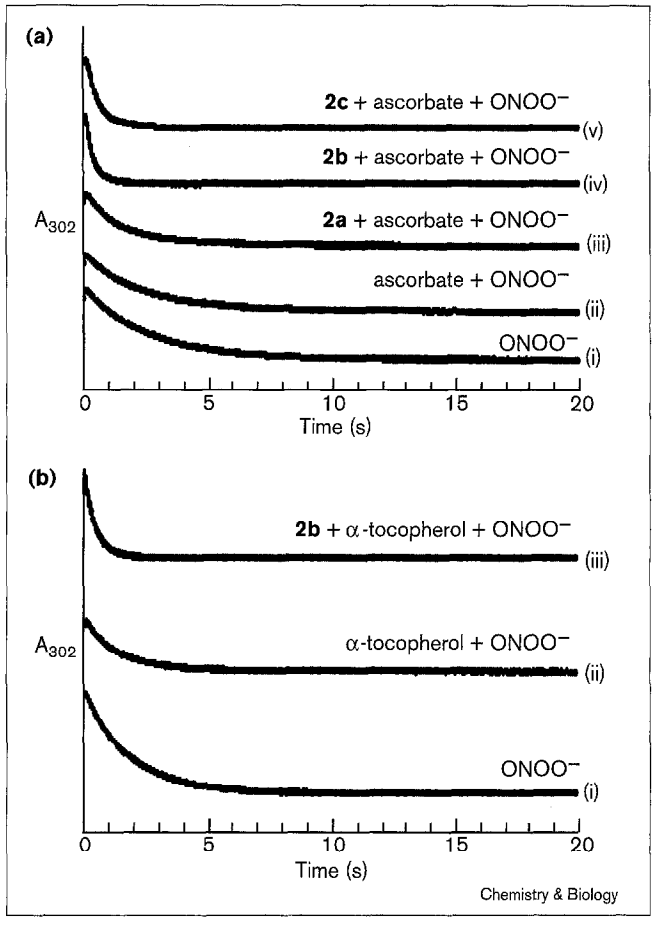

Typical kinetic profiles of the reactions of vesicular suspensions of manganese porphyrins **2a–c** with $ONOO^-$. **(a)** Decomposition of $ONOO^-$ (100 μM) monitored at 302 nm: in phosphate buffer (trace i, self-decay); in the presence of ascorbate (150 μM, trace ii); and in the presence of ascorbate (150 μM) plus 3.0 μM MnAmTPyP **(2a**, trace iii); 3.0 μM MnAmPEGTPyP (**2b**, trace iv); and 3.0 μM $MnAmPEG_6TPyP$ (**2c** trace v). The full scale corresponds to 0.6 OD. The background absorption due to porphyrin or ascorbate results in vertical displacement of traces (ii), (iii), (iv) and (v) relative to (i); all traces have been additionally offset for convenience. **(b)** Trace (i) shows the decomposition of $ONOO^-$ (75 μM) in phosphate buffer (self-decay); trace (ii) shows the reduction of $ONOO^-$ (75 μM) in the presence of α-tocopherol (83.5 μM); and trace (iii) shows the reduction of $ONOO^-$ (75 μM) in the presence of α-tocopherol (83.5 μM) plus 3.2 μM MnAmPEGTPyP (**2b**). All traces are monitored at 302 nm. The full scale corresponds to 0.4 OD. The background absorption due to porphyrin or tocopherol results in vertical displacement of traces (ii) and (iii) relative to (i). The position of trace (iii) reflects this normal vertical displacement, while trace (ii) has been additionally offset for convenience.

was completely ineffective as a reducing agent [45]. Nevertheless, as shown in Figure 8b, upon co-incorporation of α-tocopherol in phospholipid vesicles with MnAmPEGTPyP (**2b**), the decomposition of $ONOO^-$ was just as fast in the presence of α-tocopherol ($k_{cat} = 4.6 \times 10^5\ M^{-1}s^{-1}$) as in the presence of ascorbate ($k_{cat} = 5.0 \times 10^5\ M^{-1}s^{-1}$).

This porphyrin–tocopherol–lipid assembly, depicted in Figure 9, can be compared to redox-active membrane ensembles that we have designed previously [48,53,54]. For example, in a model vesicular system for biocompatible catalysis, electron transfer from a membrane-associated enzyme to the steroidal porphyrin MnChP (the iron analog of this porphyrin, FeChP, is shown in Figure 3) was mediated by an amphiphilic flavin which served as an electron shuttle [54]. In a multi-heme system for the exploration of membrane-associated electron transfer, electrons traveled through a ternary construct consisting of a cytochrome *c* recruited to the membrane surface by interaction with an amphiphilic tricarboxy Zn porphyrin (similar to FeTCAmP, shown in Figure 3) that was, in

Figure 9

MnAmPEGTPyP (**2b**) and α-tocopherol (shown in blue) self-assemble in phospholipid vesicles to form an ordered system for the catalytic reduction of $ONOO^-$. The water-soluble $ONOO^-$ reacts with the amphiphilic manganese(III) porphyrin to produce the oxomanganese(IV) porphyrin and $NO_2^{\bullet}$; the lipid-soluble biological reductant then transfers an electron to the oxoMn(IV) species, converting it back to the Mn(III) oxidation state and thus closing the catalytic cycle.

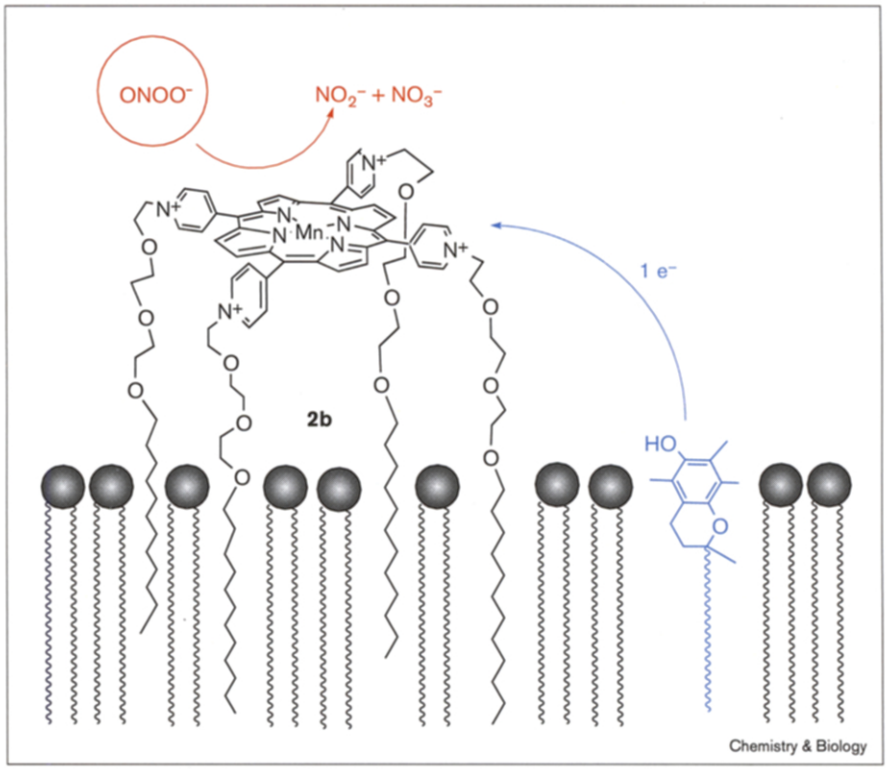

turn, tethered to a membrane-embedded MnChP [48,63]. In the present multicomponent catalytic assembly (Figure 9), the aqueous oxidant $ONOO^-$ is detoxified when it gives up its oxidizing equivalents to the membrane-bound amphiphilic manganese(III) porphyrin, producing the oxoMn(IV) porphyrin and $NO_2^{\bullet}$; the catalytic cycle is closed when the lipid-soluble α-tocopherol transfers an electron to the oxoMn(IV) species and thus converts it back to the Mn(III) oxidation state.

Peroxynitrite decomposition by metalloporphyrins bound to sterically stabilized liposomes

The amphiphilic metalloporphyrins FeAmPEGTPyP (**1b**), and MnAmPEGTPyP (**2b**) plus α-tocopherol bind to sterically stabilized liposomes (SLs), and these porphyrin–SL constructs efficiently catalyze the decomposition of $ONOO^-$. We measured the rates of $ONOO^-$ decomposition catalyzed by these porphyrin–SL constructs by monitoring the disappearance of $ONOO^-$ at 302 nm using stopped-flow spectrophotometry, as described above. We found that the **1b**–SL construct catalyzed $ONOO^-$ decomposition with a rate as rapid as the rate of $ONOO^-$ decomposition catalyzed by **1b** bound to DMPC vesicles, and that the **2b**–α-tocopherol–SL construct catalyzed $ONOO^-$ reduction at a slightly, but not significantly, slower rate than the comparable **2b**–α-tocopherol–DMPC system (see Table 1).

SLs are much more stable in biological environments than conventional phospholipid vesicles because SL formulations include phosphatidylethanolamine lipids covalently attached to long PEG chains. The enhanced stability of SLs has been attributed to the steric barrier presented to biological macromolecules by the flexible and highly mobile PEG chains [50]. The development of SLs has greatly improved the prospects for the use of liposomes in medicine [50,51]. SLs show reduced uptake by the liver and spleen and increased uptake by the gut, bone marrow and, particularly, the skin and carcass [64].

More significantly, because of their increased blood circulation time, SLs naturally extravasate to tissues where the vasculature is inherently 'leaky', resulting in accumulation of SLs at sites of tumors and inflammation [65]. SL-based cancer chemotherapy, by far the most prevalent medical application of SLs, has relied on the natural accumulation of these liposomes in tumor tissues both to deliver toxic anticancer agents, such as doxorubicin, directly to the tumors, and to protect other organs from the toxic effects of the drugs [66]. This passive targeting approach can also be applied to sites of inflammation and infection, in which the local vascular permeability is increased by the body itself, as part of the repair process [67]. Finally, SLs have recently proved amenable to active, site-specific targeting when the targeting ligands are attached to the tips of the

lipid-conjugated PEG molecules [68–70]. Thus, we anticipate that **1b**–SL and **2b**–α-tocopherol–SL could be delivered to sites of $ONOO^-$ toxicity and could therefore show activity in a variety of $ONOO^-$ related diseases.

Summary

We have designed three amphiphilic iron porphyrins **1a–c** and three amphiphilic manganese porphyrins **2a–c** that bind to liposomes and catalyze the decomposition of $ONOO^-$; the catalytic rates of these compounds are summarized in Table 1. Although the tetradodecyl pyridinium metalloporphyrins **1a** and **2a** are not particularly good catalysts, the PEG-3-linked porphyrins **1b** and **2b**, as well as the PEG-6-linked porphyrins **1c** and **2c**, are more effective by an order of magnitude. Similarly, the analogous water-soluble porphyrins FeTMPyP and MnTMPyP are more effective by an order of magnitude than the PEG-substituted porphyrins **1b–c** and **2b–c**. We conclude that this family of $ONOO^-$ decomposition catalysts performs most effectively when dissolved in aqueous solution, quite well at the interface of the lipid membrane and the bulk solution (as in compounds **1b–c** and **2b–c**), and rather poorly when tied to the surface of the lipid membrane (as in compounds **1a** and **2a**).

As potential therapeutic agents, these amphiphilic PEG-substituted metalloporphyrins have an important advantage over their water-soluble TMPyP analogs: they bind to phospholipid vesicles and thus can be administered as liposomal formulations. Liposomal delivery of the amphiphilic manganese catalysts will also allow co-delivery of these compounds with the required reducing agent, thus circumventing any possibility that the manganese porphyrins might be inaccessible *in vivo* to biological reducing agents such as ascorbate, glutathione and tocopherol.

Because of the promise that sterically stabilized liposomes have shown in a variety of biomedical applications [50–52], we have measured the rates of $ONOO^-$ decomposition by our best catalysts (**1b** and **2b**/α-tocopherol) in sterically stabilized liposomes as well as in conventional liposomes, and we concluded that these SL-bound amphiphilic porphyrins effectively catalyzed the rapid decomposition of $ONOO^-$ (see Table 1). Delivery of the amphiporphyrins in SLs may allow these drugs to circumvent potential toxicity problems, as SLs avoid rapid uptake by the liver and naturally extravasate to tumors [65] and areas of inflammation [67], both of which are potential sites of $ONOO^-$ activity [28–34]. Thus, in light of recent demonstrations that water-soluble porphyrins FeTMPyP [40,42] and MnTBAP [41,47] show activity in biological models of $ONOO^-$-related disease states, we anticipate that our new SL-bound amphiphilic $ONOO^-$ decomposition catalysts may prove to be highly effective in the chemotherapeutic treatment of any or all of the host of disease states in which $ONOO^-$ has been implicated.

Significance

Peroxynitrite ($ONOO^-$) is a potent biological oxidant that has been implicated in a large and growing array of human diseases, and there is clearly a need for drugs that can detoxify $ONOO^-$, both for further exploration and for treatment of $ONOO^-$ related diseases. We designed the amphiphilic metalloporphyrins FeAmPEGTPyP (**1b**) and MnAmPEGTPyP (**2b**) as membrane-binding analogs of known water-soluble $ONOO^-$ decomposition catalysts, and we have shown here that both compounds have significant catalytic activity in the decomposition of $ONOO^-$. The related amphiporphyrins MAmTPyP and MAmPEG$_6$TPyP (where M represents either Fe or Mn) allowed us to explore the reactivity of $ONOO^-$ in environments of varying polarity.

We have also demonstrated that the amphiphilic nature of metalloporphyrins **1b** and **2b** renders them amenable to delivery as liposomal formulations in sterically stabilized liposomes (SLs). SLs have been shown to deliver incorporated drugs to sites of inflammation and tumor; these liposomes can also be targeted to specific tissues with the addition of targeting ligands. In addition, SL delivery of drugs can potentially protect the body from toxic side effects of the drugs by reducing nonspecific uptake by the liver and spleen. Thus, the amphiporphyrin–SL constructs described here may afford powerful and flexible new strategies for the exploration and treatment of $ONOO^-$ related disease states.

Materials and methods

Materials

Tetrapyridylporphine, sodium ascorbate, tocopherol and cholesterol were purchased from Aldrich; polyoxyethylene-3-lauryl ether (**3a**), polyoxyethylene-6-lauryl ether (**3b**), and DMPC were purchased from Sigma; and PEG-2000-DSPE was purchased from Shearwater Polymers, Inc. Water used in synthetic work-up procedures was distilled; water used in all other experiments was distilled and deionized (Millipore, Milli-Q).

Analytical thin-layer chromatography (TLC) was performed using plates coated with a 0.25 mm thickness of silica gel, either with (for the iodides) or without (for the porphyrins) PF254 indicator (Analtech); plates were visualized with ultraviolet (UV) light, iodine or *p*-anisaldehyde stain. Gel-filtration chromatography was performed with Sephadex LH-20 (Pharmacia) or Sepharose 4B (Sigma).

Nuclear magnetic resonance (NMR) spectra were measured at 500 MHz on a Varian VXR500. Chemical shifts for ^{1}H NMR spectra are reported in δ units to 0.01 ppm precision with coupling constants reported in Hz to 0.1 Hz precision. Residual chloroform (δ 7.26) and DMSO (δ 2.50) were used as internal references for spectra measured in these solvents. For ^{13}C NMR spectra, residual chloroform (δ 77.0) and DMSO (δ 39.5) were used as internal standards. High-resolution and fast atom bombardment (FAB) mass spectra were measured on a Kratos MS50 mass spectrometer at the Princeton University Mass Spectrometry Facility, and electrospray mass spectra were measured on a Hewlett-Packard 5989B MS Engine. UV–visible absorbance spectra were recorded on a Hewlett-Packard HP8452A spectrophotometer. Fluorescence spectra were recorded on a Perkin-Elmer MPF66 fluorimeter. Elemental analyses were performed by Robertson Laboratories, Florham Park, NJ.

Synthesis of amphiphilic porphyrins

The amphiphilic porphyrins **6a–c** were prepared according to the method of Calvin *et al.* [58], by alkylation of TPyP (**5**) with an excess of the appropriate alkyl iodide. Representative procedures for the synthesis of alkyl iodide **4a** and for the synthesis of porphyrin **6b** from TPyP and **4a** are described below.

As noted by Meunier *et al.* [71,72], cationic porphyrins are difficult to characterize by standard methods, as their poor combustion properties often lead to large errors in elemental analyses, and their lack of volatility makes them unsuitable for FAB mass spectrometry. Electrospray mass spectrometry (ES-MS) was shown to be the best method for the characterization of tri- and tetracationic porphyrins. In addition to the above-mentioned difficulties, the alkylated pyridyl porphyrins **6a–c** demonstrated a pronounced tendency to aggregate in a wide variety of solvents, leading to complex ^{1}H and ^{13}C NMR spectra. For the tetradodecylpyridinium porphyrin **6a**, this aggregation problem was ameliorated by heating the sample to 150°C, at which temperature the peaks in the ^{1}H NMR spectrum were clearly resolved; however, even at 150°C, the PEG-substituted porphyrins **6b** and **6c** showed complex NMR spectra. Hence, although we present the ^{1}H NMR data for these compounds below, we have relied on ES-MS for the complete characterization of compounds **6a–c** (see Table 2). Our tetracationic porphyrins show characteristic [71] *m*/4, *m*-H$^+$/3, and *m*-R$^+$/3 peaks (where R is the alkyl sidechain of the alkylpyridinium group), with the *m*-H$^+$/3 most abundant for the tetradodecylpyridinium porphyrin **6a**, and the *m*-R$^+$/3 peak most abundant for the PEG-substituted pyridinium porphyrins **6b** and **6c**.

*1′-{2-[2-(2-iodoethoxy)ethoxy]ethoxy}dodecane (**4a**).* A suspension of polyoxyethylene 3-lauryl ether **3a** (1′-{2-[2-(2-hydroxyethoxy)ethoxy]ethoxy}dodecane, 1.00 g, 3.14 mmol), Ph_3P (2.47 g, 9.42 mmol), imidazole (0.64 g, 9.42 mmol), and I_2 (1.59 g, 6.28 mmol) in 60 ml of toluene was heated to reflux and stirred at this temperature for 4 h, at which point the solids had completely dissolved and TLC analysis showed no remaining starting material. The mixture was allowed to cool to room temperature; then 100 ml of saturated aqueous $NaHCO_3$ was added and the mixture was stirred for 5 min. I_2 was then added in small portions with vigorous stirring until the organic phase remained iodine-colored. Excess I_2 was then destroyed by addition of 1 M $Na_2S_2O_3$ with stirring; then the mixture was transferred to a separatory funnel and diluted with 50 ml of toluene. The phases were separated and the organic phase was washed with 50 ml of water, dried ($MgSO_4$) and concentrated by rotary evaporation. The residue was purified by flash chromatography, eluting with 4:1 CH_2Cl_2–acetone, to yield 1.08 g (80%) of the title compound as a pale yellow oil. ^{1}H NMR ($CDCl^3$) δ3.76 (t, *J* = 6.7, 2H), 3.63–3.69 (m, 6H), 3.59 (dd, *J* = 3.4, 5.5, 2H), 3.26 (t, *J* = 7.0, 2H), 1.58 (quintet, *J* = 6.7, 2H), 1.21-1.36 (m, 20H), 0.88 (t, *J* = 6.7, 3H); ^{13}C NMR ($CDCl_3$) δ 72.0, 71.5, 70.7, 70.6, 70.2, 70.0, 31.9, 29.6, 29.5, 29.3, 26.1, 22.6, 14.1, 2.8; FAB MS (*M* + 1) *m/e* calculated for $C_{18}H_{38}O_3I$ 429, found 429.

*1′-{2-[2-(2-[2-(2-iodoethoxy)ethoxy]ethoxy}ethoxy)ethoxy]ethoxy}dodecane (**4b**).* Prepared from polyoxyethylene 6-lauryl ether (**3b**), as described above, in 86% yield. ^{1}H NMR ($CDCl_3$) δ 3.75 (t, *J* = 6.7, 2H), 3.61–3.71 (m, 16H), 3.57 (dd, *J* = 3.4, 5.2, 2H), 3.44 (t, *J* = 7.0, 2H), 3.26 (t, *J* = 7.0, 2H), 1.58 (br quintet, *J* = 7.0, 2H), 1.25 (br s, 20H), 0.87 (br t, *J* = 7.3, 3H); ^{13}C NMR ($CDCl_3$) δ 71.9, 71.5, 70.5, 70.2, 70.0, 31.8, 29.6, 29.4, 29.3, 26.0, 22.6, 14.1, 2.8); HRMS (*M* + 1) *m/e* calculated for $C_{24}H_{50}O_6I$ 561.2594, found 561.2661.

*H_2AmPEGTPyP (**6b**).* To a suspension of TPyP (300 mg, 0.48 mmol) in 110 ml dimethyl formamide (DMF) was added 1′-{2-[2-(2-iodoethoxy)ethoxy]ethoxy}dodecane **4a** (3.0 g, 7.00 mmol) in 10 ml of

Table 2

Electrospray mass spectrometry data for cationic porphyrins 6a–c.

Porphyrin	Formula	MW	*m/z*	Calc'd	Obs'd
6a	$C_{88}H_{126}N_8$	1295	*m*/4	324	324
			m-H$^+$/3	432	<u>432</u>
			m-R_1^+/3	562	562
			m-H$^+$–R_1^+/2	479	479
			m-2R_1^+/2	787	787
			m-3R_1^+/1	375	375
6b	$C_{112}H_{174}N_8O_{12}$	1825	*m*/4	456	456
			m-H$^+$/3	608	608
			m-R2$^+$/3	508	<u>508</u>
			m-H$^+$–R_2^+/2	761	761
			m-2R_2^+/2	611	611
			m-3R_2^+/1	920	920
6c	$C_{136}H_{222}N_8O_{24}$	2352	*m*/4	588	588
			m-H$^+$/3	784	784
			m-R_3^+/3	639	<u>639</u>
			m-H$^+$–R_3^+/2	959	959
			m-2R_3^+/2	743	743
			m-3R_3^+/1	1052	1052

Formulas and MWs are calculated without the counter ions. R_1 represents the dodecyl sidechain of porphyrin **6a** ($C_{12}H_{25}$); R_2 represents the PEG3-dodecyl sidechain of porphyrin **6b** ($C_{18}H_{37}O_3$); R_3 represents the PEG6-dodecyl sidechain of porphyrin **6c** ($C_{24}H_{49}O_6$). For each compound, the most abundant peak is underlined.

DMF. The mixture was heated to reflux (at which point all solids were dissolved) and stirred at this temperature overnight (22 h). The mixture was allowed to cool to ~40°C; then DMF was removed by vacuum distillation at 40–60°C. The remaining red-brown slurry was applied to a Sephadex LH-20 column (5 × 40 cm), eluting with MeOH, and collecting only the red-brown porphyrin band. This fraction was resubjected to chromatography on a second Sephadex LH-20 column (5 × 25 cm), retaining only the fractions in which the UV–visible spectrum showed no extraneous peaks and the Soret maximum of the porphyrin was at 424–426 nm, to yield 1.05 g (94%) of the title compound as a shiny purple solid. ^{1}H NMR (DMSO-d6, 150°C) δ 9.44–9.58 (m, 8H), 8.88–9.15 (m, 8H), 8.19–8.23 (m, 8H), 5.18–5.26 (m, 8H), 4.30–4.40 (m, 8H), 3.80–3.90 (m, 8H), 3.48–3.76 (m, 24H), 3.32–3.46 (m, 8H), 0.98–1.72 (m, 80H), 0.78–0.92 (m, 12H), –2.75 (br s, 2H). UV–visible (50 mM phosphate buffer pH 7.4) $\lambda_{max} = 424$ nm, log $\varepsilon = 5.35$.

*H²AmTPyP (**6a**).* ^{1}H NMR (DMSO-d6, 150°C) δ 9.56 (d, $J = 6.8$, 8H), 9.15 (s, 16H), 8.97 (d, $J = 6.4$, 8H), 5.03 (t, $J = 7.32$, 8H), 2.39 (app quintet, $J = 7.3$, 8H), 1.68 (app quintet, $J = 7.3$, 8H), 1.57 (app quintet, $J = 6.8$, 8H), 1.46–1.24 (m, 56H), 0.90 (br t, $J = 6.8$, 12H); –2.80 (br s, 1.6H). *Anal.* Calculated for $C_{88}H_{126}N_8I_4$: C, 58.60; H, 7.05; N, 6.21. Found C, 58.31; H, 7.15; N, 5.94. UV–visible (50 mM phosphate buffer pH 7.4) $\lambda_{max} = 432$ nm, log $\varepsilon = 5.35$.

*H²AmPEG⁶TPyP (**6c**).* ^{1}H NMR (DMSO–d6, 150°C) δ 9.42–9.56 (m, 8H), 8.84–9.18 (m, 8H), 8.16–8.28 (m, 8H), 5.14–5.26 (m, 8H), 4.24–4.40 (m, 8H), 3.20–3.90 (m, 88H), 1.00–1.60 (m, 80H), 0.75–0.90 (br s, 12H), –2.35 (br s, 1.8H). UV–visible (50 mM phosphate buffer pH 7.4) $\lambda_{max} = 422$ nm, log $\varepsilon = 5.34$.

*Metalloporphyrins **1a–c** and **2a–c**.* The metalloporphyrins were prepared by standard methods [53] from the corresponding free-base porphyrins **6a–c**, and were used without further purification. Compounds **1a–c** showed UV–visible spectra characteristic of iron porphyrins (**1a**, $\lambda_{max} = 438$, log $\varepsilon = 4.79$; **1b**, $\lambda_{max} = 422$, log $\varepsilon = 4.81$; **1c**, $\lambda_{max} = 418$, log $\varepsilon = 4.78$), and compounds **2a–c** showed UV–visible spectra characteristic of manganese porphyrins (**2a**, $\lambda_{max} = 468$, log $\varepsilon = 4.96$; **2b**, $\lambda_{max} = 466$, log $\varepsilon = 4.96$; **2c**, $\lambda_{max} = 464$, log $\varepsilon = 4.96$).

Synthesis of ONOO–

We prepared $ONOO^-$ according to the method of Hughes and Nicklin [73], as follows. Solutions of $NaNO_2$ (0.6 M), H_2O_2 (0.6 M) acidified by HCl (0.7 M), and NaOH (0.6 M) were cooled in an ice bath for 15–30 min. The $NaNO_2$ solution (10 ml) was stirred rapidly in an ice bath, and to this solution was added the acidified H_2O_2 solution (10 ml), followed in rapid succession by the NaOH solution (10 ml). The formation of an intensely yellow solution confirmed the successful oxidation of $NaNO_2$; this yellow solution rapidly decomposed to a colorless solution in the absence of added base. Yields were maximized by precisely timing the addition of the NaOH solution, which deprotonates the unstable HOONO to produce the stable $ONOO^-$. The concentration of $ONOO^-$ was determined by measuring the UV absorbance of the solution at 302 nm ($\varepsilon = 1670 \pm 50\ M^{-1}cm^{-1}$); typical yields were 55–60%. The $ONOO^-$ solutions were stored at –20°C for up to one month, and concentrations were measured immediately prior to using the solutions. Solutions with $ONOO^-$ concentrations lower than ~80 mM were discarded.

Preparation of vesicles

Small unilamellar DMPC vesicles were prepared as follows: 10 μmol of DMPC plus the required amphiphilic porphyrin (various concentrations), and, if necessary, tocopherol (0.5 μmol), were dissolved in a small amount of chloroform in a 5-ml test tube. The chloroform was evaporated under a gentle stream of argon to form a thin film, and the film was dried for at least 3 h, and up to overnight, under vacuum. Then 3 ml of 50 mM phosphate buffer (pH 7.4) was added, and the mixture was sonicated for 10 min in a water bath (22–24°C) using a probe-tip sonicator, at which point the solution appeared transparent. The vesicular solution was allowed to equilibrate for 30 min, then centrifuged at 12,000 r.p.m. for 10 min to remove titanium dust and other particulate matter. Sterically stabilized liposomes were similarly prepared from chloroform solutions containing 10 μmol DMPC, 5 μmol cholesterol and 0.8 μmol PEG-2000-DSPE, plus the required amphiphilic porphyrin, and, if necessary, tocopherol (0.5 μmol). To confirm binding of the porphyrins to the vesicles, we performed size exclusion chromatography on Sepharose 4B of a vesicular suspension of porphyrin **1b**. Analysis of the eluting fractions by UV–visible absorbance spectroscopy showed that the porphyrin (424 nm) eluted with the lipid fraction (300 nm). Suspensions of DMPC vesicles incorporating the PEG-3 porphyrins **1b** and **2b** remained visually transparent and did not show increased scattering in the UV–visible spectra for a period of at least 12 h. Suspensions of DMPC vesicles incorporating the PEG-6 porphyrins **1c** and **2c** began to show increased scattering in the UV–visible spectra after ~2 h, and began to appear visually cloudy, indicating significant aggregation after ~3–4 h. Finally, suspensions of sterically stabilized vesicles incorporating **1b** and **2b** remained visually clear for a period of more than six months.

Reaction kinetics

Reaction kinetic profiles were collected on a HI-TECH SF-61 DX2 stopped-flow spectrophotometer in the photomultiplier mode, using single-mixing. $ONOO^-$ was monitored at 302 nm, and Mn(III) and oxoMn(IV) species were monitored at 462 and 428 nm, respectively. All reactions were conducted in phosphate pH 7.4 buffer, at a final buffer concentration of 25 mM, and at ambient temperature (22–24°C). Nonlinear least-squares fitting of the data was performed either by using the software supplied by HI-TECH or by importing the data into Kaleidagraph 3.0 for fitting.

Acknowledgements

Support of this research by the National Institutes of Health (GM36928 and RR11282 to J.T.G. for the purchase of an electrospray mass spectrometer), the National Science Foundation for the purchase of 500 and 600 MHz NMR spectrometers, and Princeton University for the purchase of a stopped-flow spectrophotometer are gratefully acknowledged. J.A.H. is the recipient of an NIH NRSA fellowship (GM18490).

References

1. Beckman, J.S., Beckman, T.W., Chen, J., Marshall, P.A. & Freeman, B.A. (1990). Apparent hydroxyl radical production by peroxynitrite: implications for endothelial injury from nitric oxide and superoxide. *Proc. Natl Acad. Sci. USA* **87,** 1620-1624.
2. Huie, R.E. & Padmaja, S. (1993). The reaction of NO with superoxide. *Free Radic. Res. Commun.* **18,** 195-199.
3. Blough, N.V. & Zafiriou, O.C. (1985). Reaction of superoxide with nitroc oxide to form peroxonitrite in alkaline aqueous solution. *Inorg. Chem.* **24,** 3504-3505.
4. Marla, S.S., Lee, J. & Groves, J.T. (1997). Peroxynitrite rapidly permeates phospholipid membranes. *Proc. Natl Acad. Sci. USA*, in press.
5. Ischiropoulos, H., *et al.,* & Beckman, J.S.(1992). Peroxynitrite-mediated tyrosine nitration catalyzed by superoxide dismutase. *Arch. Biochem. Biophys.* **298,** 431-437.
6. Beckman, J.S., *et al.,* & Tsa, M. (1992). Kinetics of superoxide dismutase- and iron-catalyzed nitration of phenolics by peroxynitrite. *Arch. Biochem. Biophys.* **298,** 438-445.
7. Floris, R., Piersma, R., Yang, G., Jones, P. & Wever, R. (1993). Interaction of myeloperoxidase with peroxynitrite. *Eur. J. Biochem.* **215,** 767-775.
8. Castro, L., Rodriguez, M. & Radi, R. (1994). Aconitase is readily inactivated by peroxynitrite, but not by its precursor, nitric oxide. *J. Biol. Chem.* **269,** 29409-29415.
9. King, P.A., *et al.,* & Suggs, J.W. (1992). A stable solid that generates hydroxyl radical upon dissolution in aqueous solutions: reaction with proteins and nucleic acid. *J. Am. Chem. Soc.* **114,** 5430-5432.
10. King, P.A., Jamison, E., Strahs, D., Anderson, V.E. & Brenowitz, M. (1993). 'Footprinting' proteins on DNA with peroxonitrous acid. *Nucleic Acids Res.* **21,** 2473-2478.
11. Radi, R., Beckman, J.S., Bush, K.M. & Freeman, B.A. (1991). Peroxynitrite-induced membrane lipid peroxidation: the cytotoxic potential of superoxide and nitric oxide. *Arch. Biochem. Biophys.* **288,** 481-487.
12. Radi, R., Beckman, J.S., Bush, K.M. & Freeman, B.A. (1991). Peroxynitrite oxidation of sulfhydryls. *J. Biol. Chem.* **266,** 4244-4250.

13. Pryor, W. A., Jin, X. & Squadrito, G. L. (1994). One- and two-electron oxidations of methionine by peroxynitrite. *Proc. Natl Acad. Sci. USA* **91,** 11173-11177.
14. Lipton, S.A., *et al.,* & Stamler, J.S. (1993). A redox-based mechanism for the neuroprotective and neurodestructive effects of nitric oxide and related nitroso-compounds. *Nature* **364,** 626-631.
15. Good, P.F., Werner, P., Hsu, A., Olanow, C.W. & Perl, D.P. (1996). Evidence for neuronal oxidation damage in Alzheimer's disease. *Am. J. Pathol.* **149,** 21-28.
16. Matthews, R.T. & Beal, M.F. (1996). Increased 3-nitrotyrosine in brains of Apo E deficient mice. *Brain Res.* **718,** 181-184.
17. Bonfoco, E., Krainc, D., Ankarcrona, M., Nicotera, P. & Lipton, S.A. (1995). Apoptosis and necrosis: two distinct events induced, respectively, by mild and intense insults with N-methyl-D-aspartate or nitric oxide/superoxide in cortical cell cultures. *Proc. Natl Acad. Sci. USA* **92,** 7162-7166.
18. Beckman, J.S., Carson, M., Smith, C.D. & Koppenol, W.H. (1993). ALS, SOD and peroxynitrite. *Nature* **364,** 584.
19. Rosen, D.R., *et al.,* & Brown, R.H. (1993). Mutations in Cu/Zn superoxide dismutase gene are associated with familial amyotrophic lateral sclerosis. *Nature* **352,** 59-62.
20. Wiedau-Pazos, M., *et al.,* & Bredesen, D.E. (1996). Altered reactivity of superoxide dismutase in familial amyotrophic lateral sclerosis. *Science* **271,** 515-518.
21. Deng, H.X., *et al.,* & Siddique, T. (1993). Amyotrophic lateral sclerosis and structural defects in Cu, Zn superoxide dismutase. *Science* **261,** 1047-1051.
22. Dawson, V.L. & Dawson, T.M. (1996). Nitric oxide neurotoxicity. *J. Chem. Neuroanat.* **10,** 179-190.
23. Szabo, C. (1996). DNA strand breakage and activation of poly ADP ribosyltransferase: a cytotoxic pathway triggered by peroxynitrite. *Free Radic. Biol. Med.* **21,** 855-869.
24. Zhang, J., Dawson, V.L., Dawson, T.M. & Snyder, S.H. (1994). Nitric oxide activation of poly(ADP-ribose) synthetase in neurotoxicity. *Science* **263,** 687-689.
25. Adamson, D.C., *et al.,* & Dawson, V.L. (1996). Immunologic NO synthase: Elevation in severe AIDS dementia and induction by HIV-1 gp41. *Science* **274,** 1917-1921.
26. Lipton, S.A. & Rosenberg, P.A. (1994). Excitatory amino acids as a final common pathway for neurologic disorders. *N. Engl. J. Med.* **330,** 613-622.
27. White, C.R., *et al.,* & Tarpey, M.M. (1994). Superoxide and peroxynitrite in atherosclerosis. *Proc. Natl Acad. Sci. USA* **91,** 1044-1048.
28. Kaur, H. & Halliwell, B. (1994). Evidence for nitric oxide-mediated oxidative damage in chronic inflammation. Nitrotyrosine in serum and synovial fluid from rheumatoid patients. *FEBS Lett.* **350,** 9-12.
29. Rachmilewitz, D., *et al.,* & Podolski, D.K. (1993). Peroxynitrite-induced rat colitis: A new model of colonic inflammation. *Gastroenterology* **105,** 1681-1688.
30. Seo, H.G., *et al.,* & Taniguchi, N. (1995). Induction of nitric oxide synthase and concomitant suppression of superoxide dismutases in experimental colitis in rats. *Arch. Biochem. Biophys.* **324,** 41-47.
31. Haddad, I.Y., Pataki, G., Hu, P., Beckman, J.S. & Matalon, S. (1994). Quantitation of nitrotyrosine levels in lung sections of patients and animals with acute lung injury. *J. Clin. Invest.* **94,** 2407-2413.
32. Mannick, E.E., *et al.,* & Coprea, P. (1996). Inducible nitric oxide synthase, nitrotyrosine, and apoptosis in *Helicobacter pylori* gastritis: Effect of antibiotics and antioxidants. *Cancer Res.* **56,** 3238-3243.
33. Douki, T., Cadet, J. & Ames, B.N. (1996). An adduct between peroxynitrite and 2′-deoxyguanosine: 4,5-dihydro-5-hydroxy-4-(nitrosooxy)-2′-deoxyguanosine. *Chem. Res. Toxicol.* **9,** 3-7.
34. Juedes, M.J. & Wogan, G.N. (1996). Peroxynitrite induced mutation spectra of PSP 189 following replication in bacteria and in human cells. *Mutat. Res.* **349,** 51-61.
35. Chan, P.H. (1996). Role of oxidants in ischemic brain damage. *Stroke* **27,** 1124-1129.
36. Huang, Z., *et al.,* & Moskowitz, M. A. (1994). Effects of cerebral ischemia in mice deficient in neuronal nitric oxide synthase. *Science* **265,** 1883-1885.
37. Szabo, C., Salzman, A.L. & Ischiropoulos, H. (1995). Endotoxin triggers the expression of an inducible isoform of nitric oxide synthase and the formation of peroxynitrite in the rat aorta *in vivo*. *FEBS Lett.* **363,** 235-238.
38. MacMillan-Crow, L.A., Crow, J.P., Kerby, J.D., Beckman, J. S. & Thompson, J. A. (1996). Nitration and inactivation of manganese superoxide dismutase in chronic rejection of human renal allografts. *Proc. Natl Acad. Sci. USA* **93,** 11853-11858.
39. Groves, J.T. & Marla, S.S. (1995). Peroxynitrite-induced DNA strand scission mediated by a manganese porphyrin. *J. Am. Chem. Soc.* **117,** 9578-9579.
40. Stern, M.K., Jensen, M.P. & Kramer, K. (1996). Peroxynitrite decomposition catalysts. *J. Am. Chem. Soc.* **118,** 8735-8736.
41. Zingarelli, B., Day, B.J., Crapo, J.D., Salzman, A.L. & Szabo, C. (1997). The potential role of peroxynitrite in the vascular contractile and cellular energetic failure in endotoxic shock. *Br. J. Pharmac.* **120,** 259-267.
42. Stern, M.K. & Salvemini, D. (1995). PCT Int. Appl. WO95/31197.
43. Salvemini, D., *et al.,* & Manning, P.T. (1996). Evidence of peroxynitrite involvement in the carrageenan-induced rat paw edema. *Eur. J. Pharmac.* **303,** 217-220.
44. Groves, J.T., Lee, J. & Marla, S.S. (1997). Detection and characterization of an oxo-manganese(V) porphyrin complex by rapid-mixing stopped-flow spectrophotometry. *J. Am. Chem. Soc.* **119,** 6269-6273.
45. Lee, J., Hunt, J.A. & Groves, J.T. (1997). Rapid decomposition of peroxynitrite by manganese porphyrin-antioxidant redox couples. *Bioorg. Med. Chem. Lett.,* in press.
46. Faulkner, K.M., Liochev, S.I. & Fridovich, I. (1994). Stable Mn(III) porphyrins mimic superoxide dismutase in vitro and substitute for it in vivo. *J. Biol. Chem.* **269,** 23471-23476.
47. Szabo, C., Day, B.J. & Salzman, A.L. (1996). Evaluation of the relative contribution of nitric oxide and peroxynitrite to the suppression of mitochondrial respiration in immunostimulated macrophages using a manganese mesoporphyrin superoxide dismutase mimic and peroxynitrite scavenger. *FEBS Lett.* **381,** 82-86.
48. Lahiri, J., Fate, G.D., Ungashe, S.B. & Groves, J.T. (1996). Multi-heme self-assembly in phospholipid vesicles. *J. Am. Chem. Soc.* **118,** 2347-2358.
49. Philipot, J.R. & Schuber, F., eds. (1995). *Liposomes as Tools in Basic Research and Industry.* CRC Press, Boca Raton, FL.
50. Lasic, D.D. & Martin, F.J. (1995). *Stealth Liposomes.* CRC Press, Boca Raton, FL.
51. Lasic, D.D. & Needham, D. (1995). The "Stealth" liposome: A prototypical biomaterial. *Chem. Rev.* **95,** 2601-2628.
52. Allen, T.M. (1996). Therapeutic opportunities for targeted liposomal drug delivery. *Adv. Drug Delivery Rev.* **21,** 117-133.
53. Groves, J.T. & Neumann, R. (1989). Regioselective oxidation catalysis in synthetic phospholipid vesicles. Membrane-spanning steroidal metalloporphyrins. *J. Am. Chem. Soc.* **111,** 2900-2909.
54. Groves, J.T. & Ungashe, S.B. (1990). Biocompatible catalysis. Enzymic reduction of metalloporphyrin catalysts in phospholipid bilayers. *J. Am. Chem. Soc.* **112,** 7796-7797.
55. Furhop, J.-H. & Mathieu, J. (1984). Routes to functional vesicle membranes without proteins. *Angew. Chem. Int. Ed. Engl.* **23,** 100-112.
56. Ungashe, S. (1991). PhD Thesis, Princeton University.
57. Marla, S.S. (1997). PhD Thesis, Princeton University.
58. Okuno, Y., Ford, W.E. & Calvin, M. (1980). An improved synthesis of surfactant porphyrins. *Synthesis* 537-539.
59. Garegg, P.J. & Samuelsson, B. (1980). Novel reagent system for converting a hydroxy-group into an iodo-group in carbohydrates with inversion of configuration. *J. Chem. Soc. Perkin I* 2866-2869.
60. Krainev, A.G. & Vainer, L.M. (1988). Penetration of ascorbic acid into bilayer phospholipid membranes. *Biokhimiya (Moscow)* **53,** 1987-1995.
61. Squadrito, G.L., Jin, X. & Pryor, W.A. (1995). Stopped-flow kinetic study of the reaction of ascorbic acid with peroxynitrite. *Arch. Biochem. Biophys.* **322,** 53-59.
62. Bartlett, D., Church, D.F., Bounds, P.L. & Koppenol, W.H. (1995). The kinetics of the oxidation of L-ascorbic acid by peroxynitrite. *Free Radic. Biol. Med.* **18,** 85-92.
63. Groves, J.T., Fate, G.D. & Lahiri, J. (1994). Directed multi-heme self-assembly and electron transfer in a model membrane. *J. Am. Chem. Soc.* **116,** 5477-5478.
64. Woodle, M.C., Newman, M.S. & Working, P.K. (1995). Biological properties of sterically stabilized liposomes. In *Stealth Liposomes.* (Lasic, D. & Martin, F., eds), pp. 103-117, CRC Press, Boca Raton, FL.
65. Huang, S.K., Martin, F.J., Friend, D.S. & Papahadjopoulos, D. (1995). Mechanism of Stealth® liposome accumulation in some pathological tissues. In *Stealth Liposomes.* (Lasic, D. & Martin, F., eds), pp. 119–125, CRC Press, Boca Raton, FL.
66. Lasic, D.D. (1996). Doxorubicin in sterically stabilized liposomes. *Nature* **380,** 561-562.
67. Bakker-Woudenberg, I.A.J.M., Storm, G. & Woodle, M.C. (1995). Stealth® liposomes as carriers of antibiotics in infectious diseases. In *Stealth Liposomes.* (Lasic, D. & Martin, F., eds), pp. 197-209, CRC Press, Boca Raton, FL.

68. Lee, R.J. & Low, P.S. (1995). Folate-mediated tumor cell targeting of liposome-entrapped doxorubicin in vitro. *Biochim. Biophys. Acta* **1233,** 134-144.
69. Allen, T.M., Brandeis, E., Hansen, C.B., Kao, G.Y. & Zalipsky, S. (1995). A new strategy for the attachment of antibodies to sterically stabilized liposomes resulting in efficient targeting to cancer cells. *Biochim. Biophys. Acta* **1237,** 99-108.
70. Huwyler, J., Wu, D. & Pardridge, W.M. (1996). Brain drug delivery of small molecules using immunoliposomes. *Proc. Natl Acad. Sci. USA* **93,** 14164-14169.
71. Bigey, P., *et al.,* & Meunier, B. (1996). Preparation and characterization by electrospray mass spectrometry of cationic metalloporphyrin DNA cleavers. *Bull. Soc. Chim. Fr.* **133,** 679-689.
72. Jakobs, A., Bernadou, J. & Meunier, B. (1997). Preparation of tetracationic metalloporphyrin-spermine conjugates. *J. Org. Chem.* **62,** 3505-3510.
73. Hughes, M.N. & Nicklin, H.G. (1970). The chemistry of peroxonitrites. Part II. Copper-catalysed reaction between hydroxylamine and peroxonitrite in alkali. *J. Chem. Soc. (A)* 925-928.